Petroleum Research 11 (2026) 1008–1020

Contents lists available at ScienceDirect

Petroleum Research

journal homepage: http://www.keaipublishing.com/en/journals/petroleum-research/

Full Length Article

Drilling wellhead structure's fire resistance evaluation with gas well blowout fires

Yudan Peng [a,*], Guodong Ji [a], Weifeng Chen [a], Binhui Liu [a], Chen Hao [a], Wenqiang Lou [b], Guangming Fu [c], Jiying Chen [d]

[a] CNPC Engineering Technology R&D Company Limited, Bejing, 102206, China
[b] Yangtze University, Wuhan, Hubei, 430100, China
[c] China University of Petroleum (East China), Qingdao, 266580, China
[d] Department of Chemical Engineering and Biotechnology, University of Cambridge, Cambridge, CB3 0AS, United Kingdom

ARTICLE INFO

Article history:
Received 6 July 2025
Received in revised form
26 January 2026
Accepted 26 January 2026
Available online 5 March 2026

Keywords:
Gas well
Blowout fire
Wellhead
Fire resistance limit
Temperature distribution

ABSTRACT

To address the absence of fire resistance evaluation methods for drilling wellhead structures under gas well blowout fires, this study firstly conducted experiments to investigate the mechanical properties of wellhead materials under high-temperature conditions. Subsequently, a temperature model and a mechanical response model of the wellhead structure under fire were established and validated respectively based on thermo-mechanical coupling methods. Furthermore, a fire resistance limit evaluation method of wellhead structures in well blowout fires was developed. The results indicated that with clearance operations at the well site, a thermal radiation threshold existed; Only when the thermal radiation exceeded this threshold, the wellhead reached its fire resistance limit and failed. Without clearance operations at the well site, the wellhead structure was certain to reach its fire resistance limit and failed. The upper surface of the wellhead had the largest displacement and reached its fire resistance limit first. The convective heat transfer coefficient, pressure load on the upper surface of the metal sealing ring, and casing gravity load had minimal influence on the fire resistance limit. Without clearance operations at the well site, the wellhead surface temperature approached the flame temperature, and the rubber seal reaches its decomposition point, leading to seal failure. The research findings could provide valuable references for the safety assessment of wellheads during gas well blowout fires and contribute to the development of effective response strategies for blowout fire control.

© 2026 Chinese Petroleum Society. Publishing services by Elsevier B.V. on behalf of KeAi Communications Co. Ltd. This is an open access article under the CC BY-NC-ND license (http://creativecommons.org/licenses/by-nc-nd/4.0/).

1. Introduction

A well blowout is a major safety incident and a primary risk control concern in oil and gas field development, characterized by the uncontrolled release of high-pressure fluids from the wellhead. A gas well blowout primarily involves methane (CH_4), which significantly elevates the risk of secondary disasters, such as blowout fires and explosions, due to its high flammability (with a lower explosive limit of 5% vol) and rapid diffusivity, causing severe harm to personnel, equipment, and the surrounding environment (Luo et al., 2021; Zhou et al., 2021). For example, the "Deepwater Horizon" well blowout and explosion accident in the Gulf of Mexico resulted in 11 deaths and 17 injuries, with economic losses of billions of dollars.

When the blowout gas is ignited, a large-scale high-temperature flame is formed, which severely challenges the safety and stability of equipment under such extreme fire conditions. The wellhead, serving as the critical interface between the surface and subsurface structures, plays a pivotal role in controlling blowout fires. Its safety and stability under fire directly influence the effectiveness of fire control and emergency response measures. In scenarios where wellsite clearance operations have not been conducted, the collapse of derricks and damage to the wellhead can obstruct gas flow, resulting in divergent flames, as shown in Fig. 1(a). In this case, the wellhead is enveloped by these flames

* Corresponding author.
E-mail address: pengyddr@cnpc.com.cn (Y. Peng).
Peer review under the responsibility of Editorial Office of Petroleum Research.

https://doi.org/10.1016/j.ptlrs.2026.01.017
2096-2495/© 2026 Chinese Petroleum Society. Publishing services by Elsevier B.V. on behalf of KeAi Communications Co. Ltd. This is an open access article under the CC BY-NC-ND license (http://creativecommons.org/licenses/by-nc-nd/4.0/).

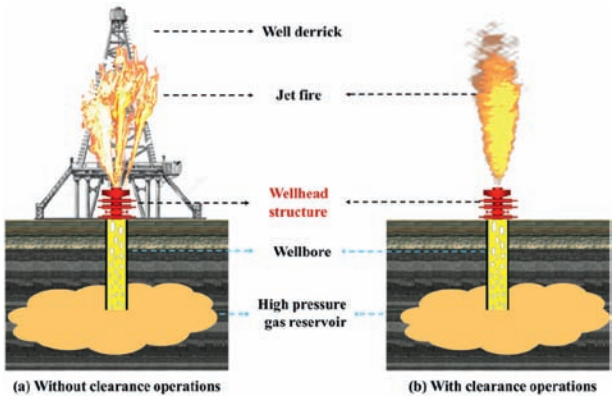


Fig. 1. Well blowout fire.

with intense thermal radiation and convective heating. Conversely, when clearance operations are performed, the gas forms a jet flame, with the wellhead primarily affected by thermal radiation, as shown in Fig. 1(b). The fire resistance limit is a key metric for evaluating structural stability and safety in fires, which is defined as the duration a structure can withstand fire exposure while maintaining stability, integrity, and insulation. Research on the fire resistance limit of wellhead structures under blowout fire can provide valuable insights for evaluating their safety and stability, and is crucial for reducing the risk of blowout fires and implementing effective response measures.

The blowout flame is essentially a jet fire Research has been conducted on jet fire and structural safety under fire. However, research on the mechanical response characteristics, temperature field distribution, and fire resistance limit of wellhead structures under high-temperature gas well blowout fires remains limited, and methods for evaluating the safety of wellhead structures under such conditions are lacking, which poses a risk to the disposal of blowout fire.

The development of compartment fire was simulated with FDS by Hao (2020), and the sequential thermo-mechanical coupling method was applied to calculate the thermal response and residual strength of deck structures at elevated temperatures. Lv (2018) combined numerical simulation and experimental techniques to establish temperature field models and fire resistance limit models for concrete-filled steel tube columns under fire conditions, along with a model for calculating the residual load-bearing capacity after a fire. He et al. (2019, 2020a, 2020b) conducted studies on the post-fire residual bearing capacity of hollow steel columns and concrete-filled steel tube columns with experimental and numerical simulation methods. The accuracy of the numerical models in calculating the residual bearing capacity of steel tubes post-fire was demonstrated, and the results were compared with standards such as Eurocode EN 1993-1-4, SEI/ASCE-8, and AS/NZS 4673, which were shown to be conservative in predicting axial compressive strength after fire exposure. The failure stress of corroded pipelines under high-temperature fire conditions was analyzed by Wang and Qiao (2020) using ANSYS software, revealing that elevated temperatures alter the material properties and stress states around defects, reducing the residual strength of the pipelines. Wang (2021) and Sheng (2021) investigated the mechanical behavior of concrete-filled steel tube short columns after fire exposure, establishing numerical models for temperature fields and axial pressure in steel columns under high temperatures. The impact of various parameters on column stability was analyzed, and simplified formulas for calculating residual strength were proposed. Duan et al. (2017) developed a thermo-mechanical coupling analysis method for steel structures under fire using FDS and ABAQUS, which was validated against real-world cases, confirming its accuracy. Lu, 2021 used a numerical simulation method to develop fire resistance limit models for void-layered concrete-filled steel tubes under normal, heating, and cooling conditions, and the influence of various parameters on fire resistance was analyzed. Qi (2011) conducted numerical simulations on the temperature field, fire resistance limits, and residual load-bearing capacity of reinforced concrete columns, beams, and frame structures under fire conditions. Ma (2018) and Yu (2019) established a shear strength calculation model for reinforced concrete beams under fire with ABAQUS, analyzing the shear strength and fire resistance limits under different fire conditions. A temperature field model for a drilling blowout preventer during a blowout fire was developed by Shi and Liu (2019) using ABAQUS, and the temperature distribution under fire conditions was analyzed. Zhang (2019) developed a fully coupled thermo-fluid-structural model for a thermal recovery wellhead, where thermal recovery temperatures reached 338 °C, significantly increasing deformation under thermal loads. This finding indicated that thermal-induced stress must be considered in strength assessments. Zhou et al. (2023) used FDS software to create a thermal response analysis model for petrochemical pipelines under pool fire conditions, and a temperature rise formula for pipelines was developed. Foroughi et al. (2021) conducted experimental studies on the impact of sonic jet flames formed by pipeline leaks on adjacent pipelines, demonstrating that air-filled pipelines reached 800 °C after 9 min of flame exposure, while pipelines containing water exhibited slower temperature rises, with maximum temperatures reaching 150 °C. Fan et al. (2016) investigated the compressive behavior of unrestrained stainless steel columns under fire through experiments, revealing that load ratio and eccentricity were key factors influencing critical temperature and fire resistance. Rodrigues and Laím, 2019, and Tondini et al. (2013) performed experiments on hollow stainless steel columns with rectangular and circular cross-sections under compressive loads, identifying failure deformation modes and calculating fire resistance limits and failure temperatures. The fire performance of axially and eccentrically loaded steel columns has also been examined through both experimental and numerical methods, highlighting the influence of various parameters on fire resistance and resulting in the development of buckling temperature prediction models (He, 2018; Li, 2015; Sun, 2016). In addition, research on Q960, Q460, and Q690 steel beams under fire conditions has analyzed their thermal response characteristics and produced buckling temperature formulas to support fire-resistant design (Ge, 2012; Xia, 2018; Zhang, 2022). Experiments were also conducted to study the mechanical properties of wellhead materials under high temperature conditions. A temperature model and a mechanical response model of the wellhead structure under fire were established and validated respectively based on thermo-mechanical coupling methods. And a fire resistance limit evaluation method of wellhead structures in well blowout fires had been developed. The research findings could provide valuable references for the safety assessment of wellheads during gas well blowout fires and contribute to the development of effective response strategies for blowout fire control.

2. Wellhead and casing material's high temperature mechanical properties

The wellhead structure comprises the wellhead, shallow casing, and metal and rubber seals, as illustrated in Fig. 2. The mechanical properties of wellhead structural materials at high temperatures form the basis for analyzing the fire resistance limits of the

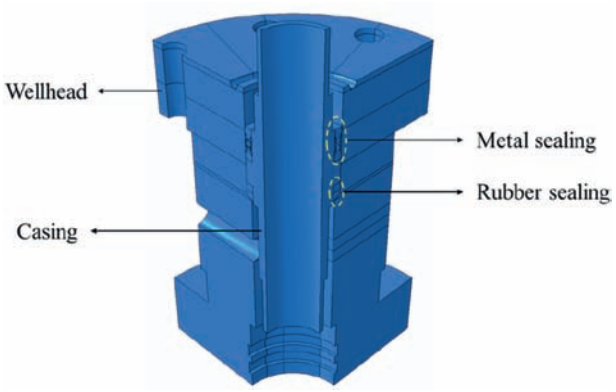


Fig. 2. Wellhead structure.

wellhead structure. While the mechanical properties of high-temperature metal sealing materials (316L) and rubber sealing materials have been extensively studied, these properties will be introduced in the next section. However, there has been limited research on the high-temperature mechanical properties of wellhead materials (35CrMo) and casing materials (N80). Therefore, high-temperature mechanical property experiments were conducted for the wellhead and casing materials to obtain stress–-strain curves, yield strength, elastic modulus, ultimate tensile strength, and elongation rates at elevated temperatures.

2.1. Experimental setup and method

The wellhead and casing materials were machined using the Vturn-S26/110 precision machining instrument manufactured by Taichung Precision Machinery. The specimen dimensions were shown as following Fig. 3 (a). High-temperature mechanical property tests on the wellhead and casing materials were conducted using a microcomputer-controlled electronic universal testing machine (UTM05HB) produced by Sansi Zongheng, as shown in Fig. 3 (b). The testing machine had a maximum test capacity of 100 kN, with a load control accuracy of ±0.5%. During the high-temperature tensile tests, a high-temperature furnace was installed in the middle of the testing machine to heat the specimens. The furnace utilizes electric heating wires to achieve

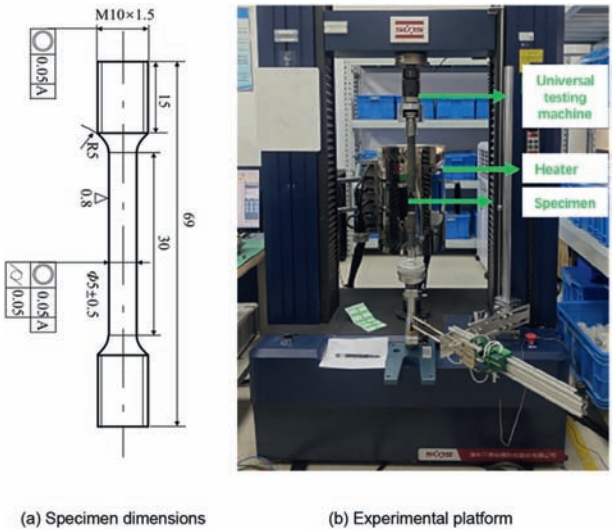


Fig. 3. Specimen dimensions and Experimental platform.

temperatures ranging from 300 °C to 1100 °C, allowing the specimens to reach the preset test temperatures with a temperature control accuracy of ±1%. For the high-temperature tensile tests of the wellhead and casing materials, multiple temperature points were selected: 20 °C, 400 °C, 500 °C, 600 °C, and 700 °C. Each test was repeated three times under the same conditions.

During the experiment, the high-temperature furnace was used to heat the specimens at a preset heating rate of 20 °C/min to the target temperature, where the temperature was then maintained for 30 min. During the heating and holding process, the load on the testing machine was kept at zero to allow the specimens to expand naturally without any external force. At the beginning of the experiment, the loading rate was set at 0.1 mm/min until the specimen deformation reached 2.0 mm. In the second stage, the loading rate was increased to 1.0 mm/min and maintained until the specimen fractured. Throughout the experiment, the temperature remained constant.

2.2. Experimental results

2.2.1. Mechanical properties of wellhead structure materials at high temperatures

Mechanical properties of the wellhead material at different temperatures were shown in Fig. 4. The influence of temperature on the material's mechanical performance was evident. As shown in Fig. 4(a), stress values at the same strain decrease progressively with increasing temperature. This reduction is particularly pronounced between 20 °C and 400 °C, as well as between 500 °C and 600 °C, indicating a significant decline in mechanical properties within these temperature ranges. Fig. 4(b)–4(f) illustrated the effects of temperature on elastic modulus(E), yield strength ($\sigma_{0.2}$), tensile strength (σ_u), ultimate load (F), and elongation (d). Except for elongation, all mechanical parameters showed a notable decrease with rising temperature. Compared to 20 °C, the elastic modulus, yield strength, tensile strength, and ultimate load decreased by 89.5%, 92.2%, 92.0%, and 89.02%, respectively, while elongation increased by 373.7%.

2.2.2. Mechanical properties of casing materials at high temperatures

Mechanical properties of casing materials at different temperatures are shown in Fig. 5. As shown in Fig. 5(a), stress at a constant strain level gradually decreased with increasing temperature. This reduction was particularly pronounced within the temperature ranges of 20 °C–400 °C, 400 °C–500 °C, and 500 °C–600 °C, indicating a significant decline in mechanical performance. Furthermore, the effects of temperature on the elastic modulus, yield strength, tensile strength, ultimate load, and elongation rate of the casing materials were shown in Fig. 5. Except for the elongation rate, all mechanical parameters exhibited a substantial decreasing trend with increasing temperature. Compared to 20 °C, the elastic modulus, yield strength, tensile strength, and ultimate load decreased by 88.7%, 93.0%, 93.1%, and 88.4%, respectively, while the elongation rate increased by 477.3%。

3. Wellhead structure material's thermal properties with fires

The thermal parameters of wellhead structural materials were the basis for calculating temperature field. The wellhead structure consisted of a wellhead, casing, metal sealing ring, and rubber sealing ring, with materials of 35CrMo, N80, 316L, and rubber, respectively. N80, 35CrMo, and 316L were all steel materials with similar thermal properties.

The thermal conductivity model, thermal expansion coefficient model and specific heat capacity model for steel under fire

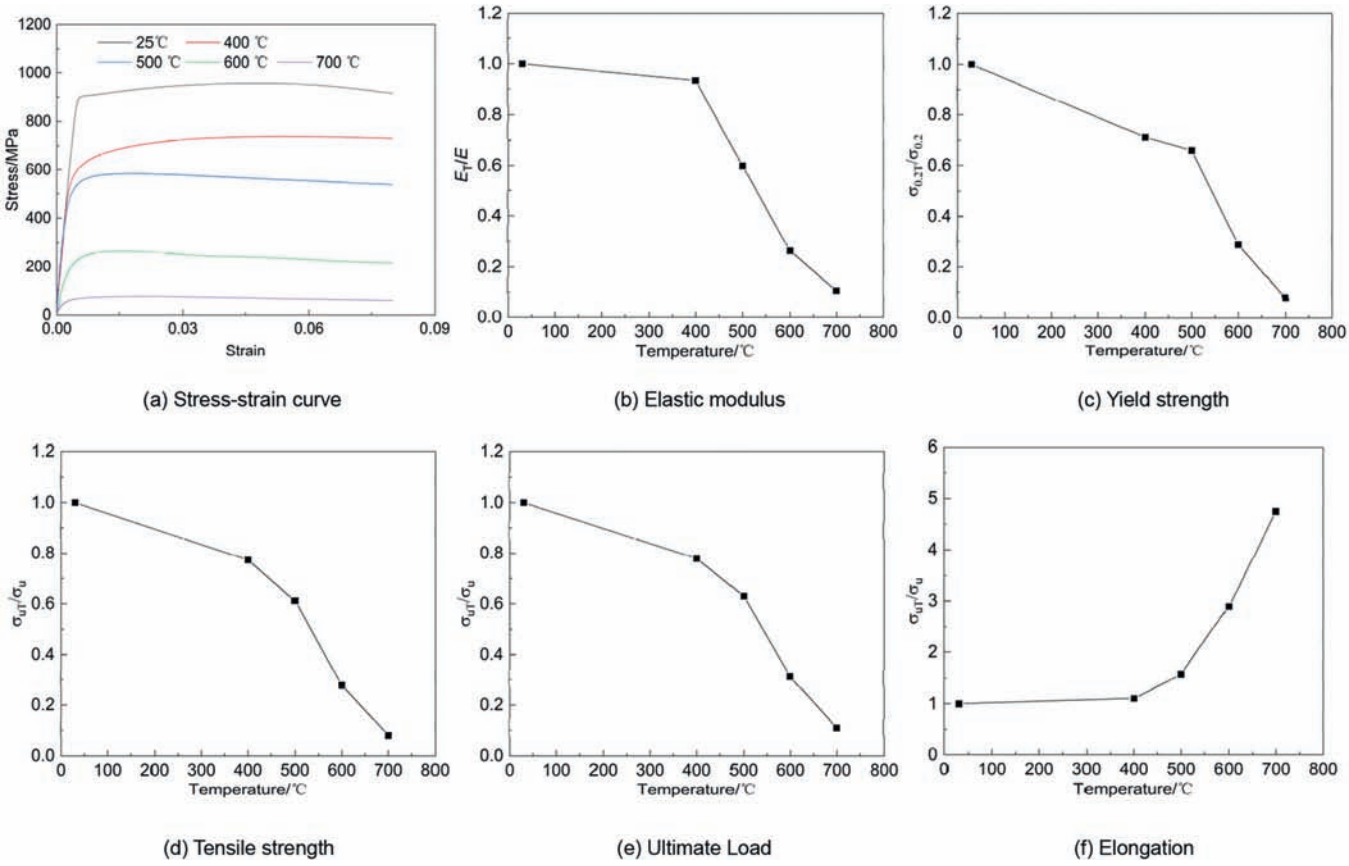


Fig. 4. Mechanical properties of wellhead materials at different temperatures.

conditions, as specified in the European Eurocode 3 standard (CEN, 2005), are employed:

$$\lambda = \begin{cases} -3.33 \times 10^{-2} T_f + 54 & 20^\circ C \le T_f \le 800^\circ C \\ 27.3 & 800^\circ C \le T_f \le 1200^\circ C \end{cases} \quad (1)$$

where, λ is the thermal conductivity of steel, W·m^{-1}·°C; T_f is the temperature of the steel, °C.

$$\alpha = \begin{cases} 0.8 \times 10^{-8}\left(T_f - 20\right) + 1.2 \times 10^{-5} & 20^\circ C \le T_f < 750^\circ C \\ 0 & 750^\circ C \le T_f < 860^\circ C \\ 2.0 \times 10^{-5} & 860^\circ C \le T_f < 1200^\circ C \end{cases} \quad (2)$$

Where, α is thermal expansion coefficient of steel.

$$c = \begin{cases} 2.22 \times 10^{-6} T_f^3 - 1.69 \times 10^{-3} T_f^2 + 7.73 \times 10^{-1} T_f + 425 & 20^\circ C \le T_f < 600^\circ C \\ 666 + 13002 \Big/ \left(T_f - 738\right) & 600^\circ C \le T_f < 735^\circ C \\ 545 + 17820 \Big/ \left(T_f - 731\right) & 735^\circ C \le T_f < 900^\circ C \\ 650 & 900^\circ C \le T_f < 1200^\circ C \end{cases} \quad (3)$$

Where, c is the specific heat capacity of steel.

The density and Poisson's ratio of steel exhibit minimal variation with temperature. Eurocode 3 adopts constant values (CEN, 2005), specifically a density of 7850 kg m^{-3} and a Poisson's ratio of 0.3. The mechanical properties of N80 casing materials and 35CrMo wellhead materials at elevated temperatures are obtained from the experimental data presented in the previous section. After data processing, the mechanical properties data of these materials at high temperatures are imported into ABAQUS for further analysis. The metal sealing material is 316L stainless steel, and its mechanical properties at various temperatures are shown in Fig. 6 (Blandford et al., 2007; Gibbs and Wyatt, 1961).

The sealing between the wellhead and the casing hanger adopted the commonly used metal and rubber sealing structure on site. The mechanical properties of rubber under high-temperature conditions were complex. The results show that when the temperature of rubber in fire was less than 200 °C, it does not decompose obviously; The temperature of rubber was 250 °C–300 °C, and the quality of rubber began to decline; The temperature of rubber is more than 300 °C, and its residual mass

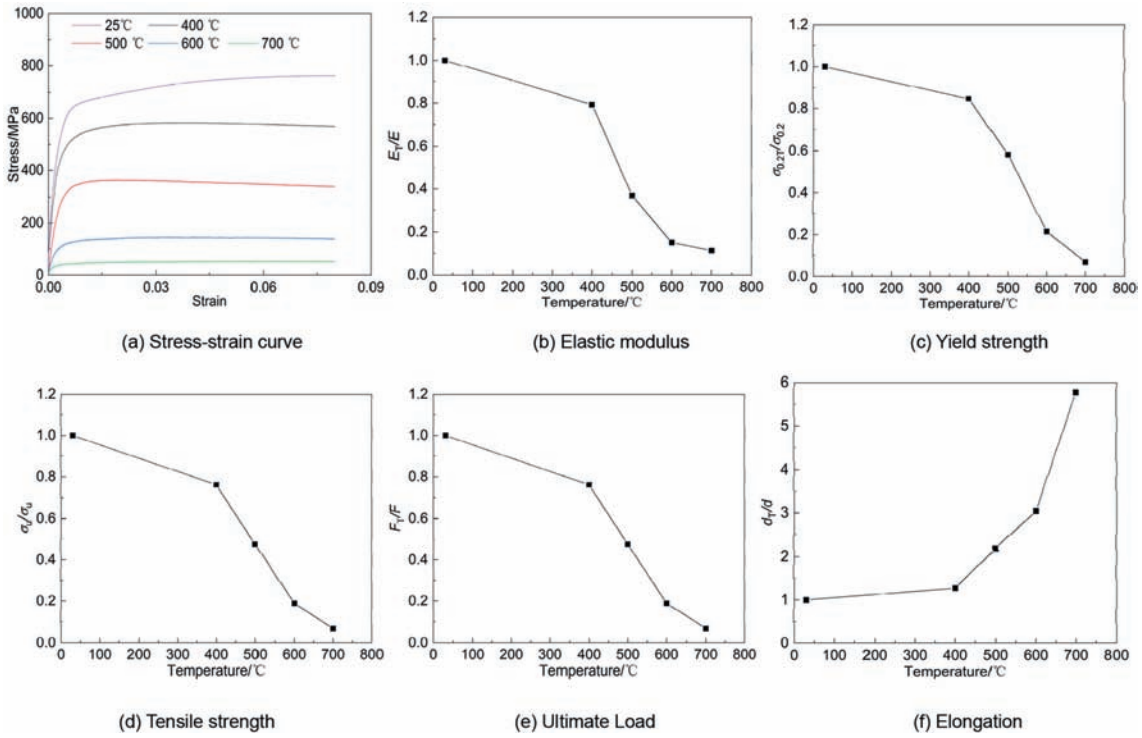


Fig. 5. Mechanical properties of casing materials at different temperatures.

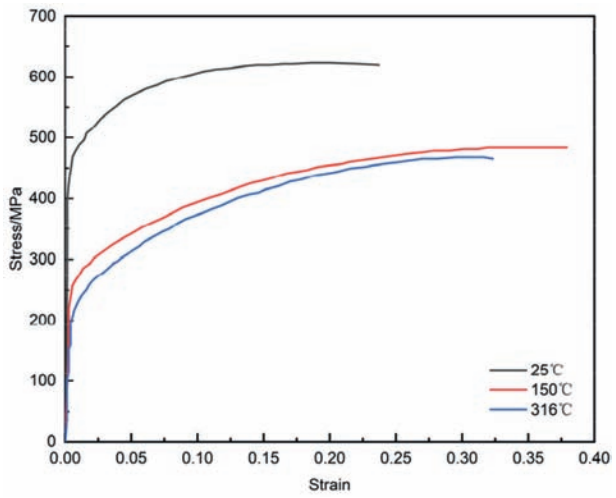


Fig. 6. Stress-strain curves of 316L material at different Temperatures (Blandford et al., 2007; Gibbs and Wyatt, 1961).

decreases rapidly, resulting in a significant reduction in its mechanical properties (Wang and Guan, 2019). Zhou (2015) and Fang's (2006) measured the thermal conductivity, specific heat, expansion coefficient, and density of rubber under high temperature, as well as the mechanical parameters. These parameters were used in this study.

4. Wellhead structure's temperature field under well blowout fires

4.1. Temperature field theory

4.1.1. Convective heat transfer

Under obstruction-free conditions, convective heat transfer primarily consists of heat transfer from the flame to the outer wall of the wellhead and from high-velocity gas to the inner wall of the casing. In obstruction-cleared conditions, convective heat transfer is mainly from high-velocity gas to the inner wall of the casing. The convective heat transfer equation is presented below (Lv, 2018).

$$Q_c = h\cdot(T_c - T_s) \tag{4}$$

Where, Q_c is the convected heat transfer, $W\cdot m^{-2}$; h is the convective heat transfer coefficient, $W\cdot m^{-2}\cdot{}^{\circ}C^{-1}$; T_c is the temperature of the convective fluid, °C; Ts is the temperature of the solid surface, °C.

4.1.2. Radiation heat transfer

Under well-blowout fire conditions, radiation heat transfer includes the transfer between the flame and the outer wall of the wellhead, as well as between the internal structures of the wellhead and the surrounding air. Additionally, under obstruction-cleared conditions, the primary heat source is the radiation from the flame to the wellhead. The radiation heat transfer equation is presented below (Lv, 2018).

$$Q_r = \chi_r\cdot\sigma\cdot\left[(T_c+273)^4 - (T_s+273)^4\right] \tag{5}$$

Where, Q_r is the radiation heat transfer, $W\cdot m^{-2}$; χ_r is comprehensive radiation coefficient; σ is Stefan Boltzmann constant, $5.67\times10^{-8}\ W\ m^{-2}\ K^{-4}$.

4.1.3. Heat conduction

Heat conduction involves the transfer of heat between the wellhead and the sealing structure, between the wellhead and the casing, and between the sealing structure and the casing. The heat conduction within the wellhead structure during a fire is a process of three-dimensional transient heat transfer. The heat conduction

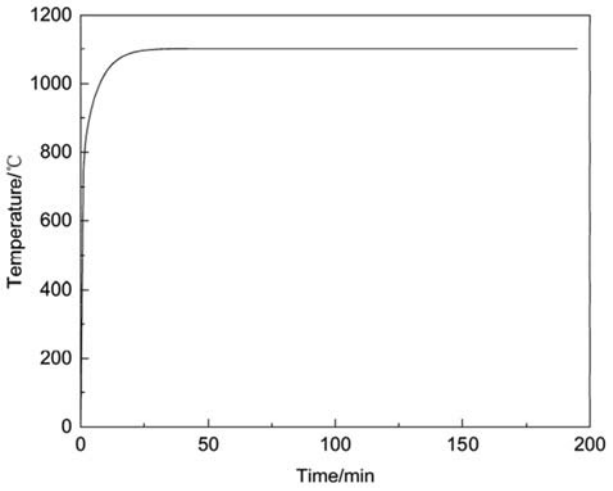


Fig. 7. Heating curve of hydrocarbon fuel fire (Sheng, 2021).

equation is as follow (Lv, 2018):

$$\rho c\frac{\partial T}{\partial t}=k\left(\frac{\partial^2 T}{\partial x^2}+\frac{\partial^2 T}{\partial y^2}+\frac{\partial^2 T}{\partial z^2}\right) \tag{6}$$

Where, ρ is the density of the material, kg·m^{-3}; c is the specific heat capacity at constant pressure, J·kg^{-1}·°C^{-1}; k is the thermal conductivity, W·m^{-1}·K^{-1}; t is time, s.

4.2. Temperature field model establishment

Based on the aforementioned theories, material thermal parameters, and the ABAQUS, a finite element model of the temperature field for the wellhead structure under blowout fire conditions was established. Due to the geometric symmetry of the model, only one-quarter of the geometric model was analyzed, as shown in Fig. 7. Without clearance operations at the well site, the primary heat source is the convective heat transfer from the flame to the outer surface of the wellhead. The main component of the blowout flame's fuel is methane (CH_4). Therefore, the temperature rise curve for the blowout fire without clearance operations at the well site follows the hydrocarbon fuel temperature rise curve (Lv, 2018), as shown in Fig. 7. The model was meshed using DC3D8 thermal conduction elements. A sensitivity analysis of mesh density was conducted by selecting four critical temperature nodes in the model, as shown in Fig. 8. The results indicated that when the mesh count reached 170,000, the temperature of different nodes stabilized after 3 h of fire exposure. Therefore, the optimal mesh count for the model was determined to be 170,000. The initial temperature field of the model was set to 20 °C, and the contact surfaces between the wellhead and internal structures were defined using tie constraints. The model utilized the Heat Transfer transient analysis step. For the exposed surface, the convective heat transfer coefficient was set to 50 W m^{-2} K^{-1}, and the radiation coefficient was set to 0.5. For the back surface, the convective heat

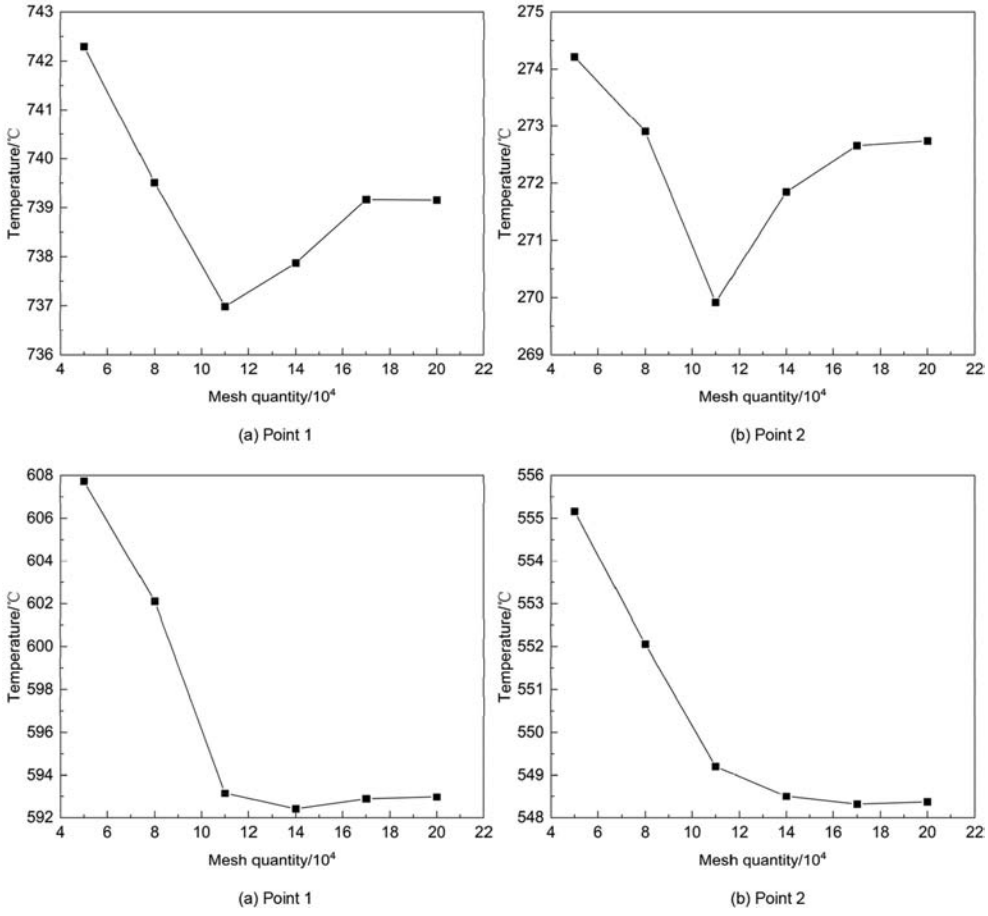


Fig. 8. Mesh sensitivity analysis.

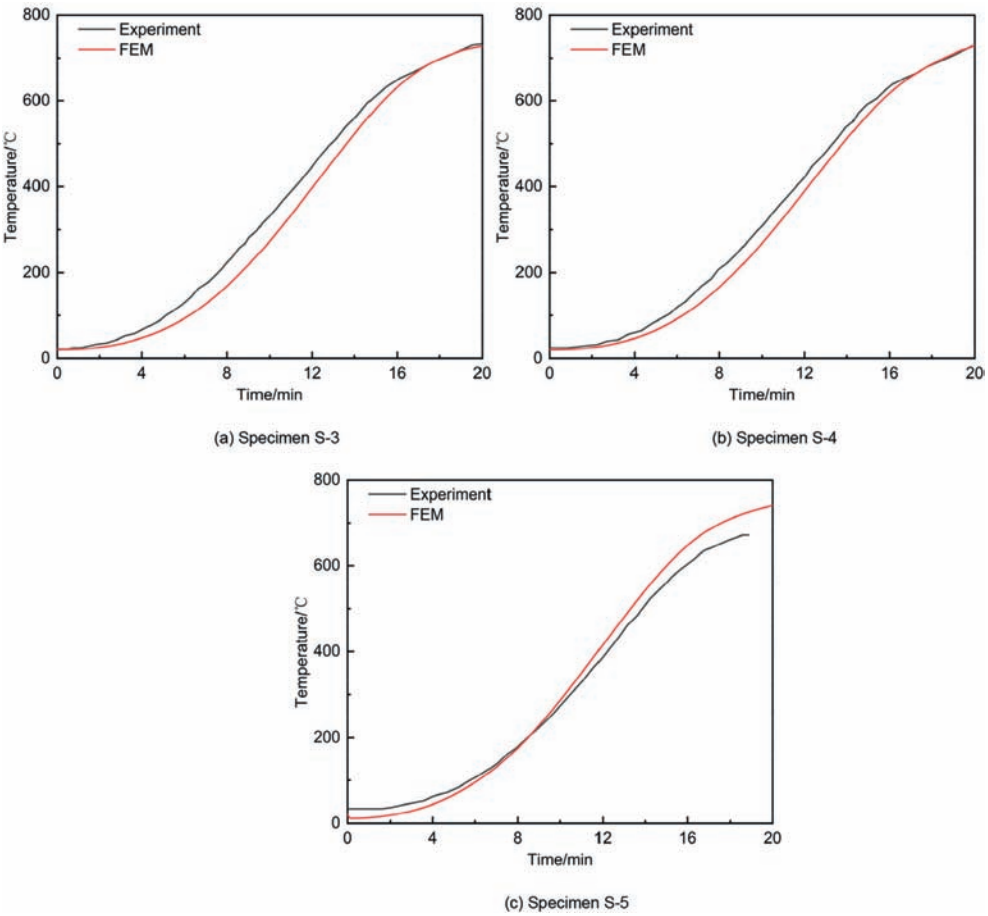


Fig. 9. Experimental and numerical simulation results of steel beam temperature.

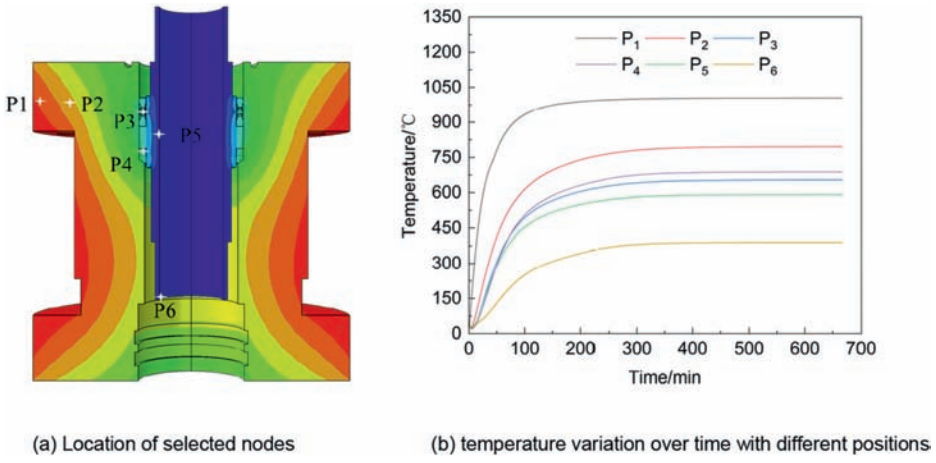


Fig. 10. Location of selected nodes and theirs temperature.

transfer coefficient was set to 9 W m^{-2} K^{-1}, with a radiation coefficient of 0.5. With clearance operations at the well site, the temperature field model applies a heat flux load generated by thermal radiation in ABAQUS load module, and the convective heat transfer from the flame to the wellhead in the contact settings module is removed. And other parameters remain unchanged.

4.3. Temperature field model validation

Due to the significant challenges of conducting fire tests on wellhead structures and the limited availability of relevant experimental data, the temperature field model and parameter selection in this section were validated using published

experimental data on steel beams under fire conditions. Zhang (2022) conducted experiments measuring the temperature distribution of steel beams at various locations during fire exposure. These data were used to verify the validity of the simulation approach and parameter choices. The measured temperatures of the three steel beam specimens under fire conditions, along with the temperatures simulated using the methods and parameters described in this section, are shown in Fig. 9. As shown in Fig. 9, the measured temperature curves of the three steel beam specimens during the fire closely match the simulated temperature curves over time. This consistency indicates that the temperature field simulation approach and parameter selection in this study are reasonable.

4.4. Wellhead structure's temperature field analysis during well blowout fires

4.4.1. Wellhead structure's temperature field without clearance operations at the well site

Without clearance operations at the well site, the wellhead structure is surrounded by flames and subjected to high temperatures, as shown in Fig. 1(a). The parameters that influence the temperature distribution in the structure during a blowout fire include the fire temperature rise curve, the convective heat transfer coefficient and radiation coefficient on the fire-exposed surface, the convective heat transfer coefficient and radiation coefficient on the back surface, as well as the convective heat transfer coefficient and gas temperature affecting the inner wall of the casing. In those parameters, the convective heat transfer coefficient and gas temperature on the inner wall of the casing vary according to the blowout conditions, while the other parameters are taken as specified in Section 4.2.2.

Using a convective heat transfer coefficient of 0.1 kW m^{-2} K^{-1} and a gas temperature of 50 °C as an example, the temperature variation of the wellhead structure over time was analyzed. Node locations within the structure are shown in Fig. 10, along with their temperature response curves during the fire. The results indicate that temperatures at all node positions initially rise sharply and then stabilize, exhibiting similar trends. Node P1 (located on the wellhead) reaches a stable temperature earliest, around 200 min into the fire. This is due to its proximity to the fire-exposed surface and its distance from the convective heat transfer zone near the inner casing wall. P1 is primarily influenced by the flame temperature with minimal effect from convective heat transfer, allowing for quicker stabilization. It also attains the highest temperature among all nodes, stabilizing at 1000 °C, slightly below the temperature specified in the fire curve. Node P2, being farther from the fire-exposed surface, has a lower temperature than P1. The temperature at P3 (metal seal) stabilizes at a lower value than both P1 and P2, as well as P4 (rubber seal). This is because P3 (metal) has no direct thermal conduction with the wellhead wall, unlike P4 (rubber). Nodes P5 and P6, located at the casing hanger, are directly affected by convective heat transfer from the gas flow. P5, being closer to the contact surface between the casing hanger and the wellhead, has a higher temperature than P6, with heat transferring from P5 to P6 as the fire progresses.

4.4.2. Wellhead structure's temperature field with clearance operations at the well site

With clearance operations at the well site, the gas jet from the wellhead forms a unidirectional jet flame that does not directly impinge on the wellhead, as illustrated in Fig. 1(b). Under these conditions, the primary heat source for the wellhead structure is thermal radiation from the flame. The temperature variations at different locations within the wellhead structure over time are presented in Fig. 11. In this scenario, the convective heat transfer coefficient is 6 kW m^{-2} K^{-1}, the gas temperature is 100 °C, and the thermal radiation intensity is 30 kW m^{-2}. The node positions are indicated in Fig. 10. As shown in Fig. 11, temperatures at various positions within the wellhead structure initially rise with increasing fire duration and then stabilize. Position P1 (wellhead surface) reaches the highest temperature, approximately 550 °C, followed by position P2. This is primarily because N1 is closest to the wellhead surface (the area directly exposed to thermal load). P1 and P2 stabilize at similar times. The temperature at position N4 (rubber seal) is slightly higher than at position P3 (metal seal). Although P3 and P4 are at similar distances from the radiation source and the convective heat transfer surface, P4 has direct thermal conduction with the wellhead, resulting in a higher temperature. And both positions take longer to reach temperature stabilization compared to P1 and P2. Position P5 (casing) exhibits a lower temperature than P3 due to its proximity to the inner wall of the casing, where convective heat transfer effects are more pronounced. Position P6, also near the inner casing wall, records the lowest temperature. Despite P5 and P6 being at similar distances from the inner wall of the casing hanger, P5 has direct thermal conduction with the wellhead. Additionally, P5 and P6 reach stable temperatures more quickly than other positions, indicating that thermal radiation from the wellhead surface has a minimal impact on their temperatures under these conditions.

5. Wellhead structure's fire resistance limit

Based on the temperature field model of the wellhead structure and the obtained material thermal parameters, thermo-mechanical coupling models were established with and without the condition of clearance operations at the well site. The fire resistance limits and displacement response patterns under different conditions were analyzed.

5.1. The thermo-mechanical coupling model's establishment

A thermo-mechanical coupling model of the wellhead structure was developed using ABAQUS software. The geometric model utilized a 1/4 symmetry model due to its symmetrical characteristics. From the temperature field analysis in the previous section, it is evident that the temperature at the rubber sealing position exceeds its decomposition temperature under obstruction-free conditions, leading to rubber decomposition and failure. Additionally, clearing operations at the well site during a blowout fire are time-consuming, and the rubber seals are typically burned out. For example, in the blowout fire incident at Well X in Western China, the rubber sealing rings were found destroyed after cutting the wellhead. Furthermore, simulating the decomposition of the rubber seal under high temperatures in the thermo-mechanical coupling analysis presents significant challenges. And the dimensions of the sealing ring are negligible compared to those of the entire wellhead structure. Therefore, it is assumed that the rubber has decomposed under high-temperature fire conditions, and the effect of the rubber ring is neglected.

A sequential thermo-mechanical coupling method was employed to analyze the mechanical response characteristics of the structure under high-temperature fire conditions. Specifically, the temperature field of the structure was solved first, and then the nodal temperatures were applied to the structural model to compute its mechanical response. During the mechanical analysis, C3D8R element was adopted. This type of element maintains high accuracy in displacement and stress calculations even when the

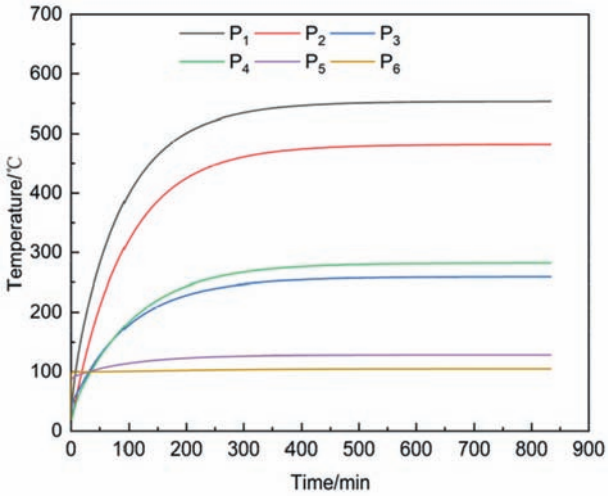


Fig. 11. Wellhead's different positions temperature.

mesh undergoes significant distortion. The model included two static general analysis steps to apply mechanical and thermal loads. The boundary conditions and loads of the model are shown in Fig. 12. Symmetry constraints were applied to the two symmetrical surfaces, and a fixed support constraint was applied at the bottom of the wellhead. A pressure load F_1 was applied to the upper end face of the metal sealing pressure ring. A pressure load F_2 was applied to the upper end face of the wellhead. A load F_3 was applied at the bottom of the casing. Contact interactions were defined at the interfaces where components of the wellhead structure are in contact. In engineering practice, the following criterion is commonly used to determine whether a structure has reached its fire resistance limit: the vertical deformation of the structure reaches 1% of the dimension of the fire-exposed structural component (Lv, 2018).

5.2. Model validation

The fire resistance limit is defined as the duration of fire exposure corresponding to the point at which a structure reaches its ultimate displacement. Due to the complexity and large size of the wellhead structure, conducting relevant fire tests and measuring deformations is highly challenging. Therefore, displacement response data of steel beams under fire were used to validate the structural fire resistance calculation model and parameter selection established in this study. Zhang (2022) conducted experimental research on steel beam structures under fire, measuring displacement responses under various fire scenarios. The finite element model of steel beam displacement response under fire, developed based on these methods and parameters, was compared with the experimentally measured displacement values, as shown in Fig. 13. As shown in Fig. 13, the numerical simulation results of mid-span displacements for the three specimens under fire conditions closely match the experimental data. For specimens S-3, S-4, and S-5, the difference between the simulated and experimental values are more significant during the fire exposure time of 400–700 min. However, for exposure times of 0–400 min and times greater than 600 min, the difference between simulated and experimental values are relatively small. The average difference between the experimental results and numerical simulations for specimens S-3, S-4, and S-5 are 19.0%, 15.26%, and 10.25%, respectively. Considering measurement difference and other uncertainties, the model established using these methods and parameters reasonably reflects the

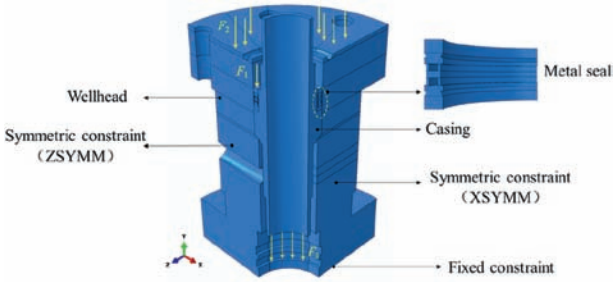


Fig. 12. Wellhead thermal-mechanics coupling model.

experimental result. This indicates that the approach to simulate the displacement response of the wellhead structure under fire conditions and the selection of parameters are reasonable.

5.3. Wellhead structure's displacement response under well blowout fires

Analysis results indicate that the displacement of the wellhead structure at high temperatures during a fire occurs primarily in the vertical direction (U2 direction), while changes in the horizontal directions (U1 and U3) are minimal. Since the criterion for determining the fire resistance limit focuses on the vertical displacement of the structure, the vertical displacement under different operating conditions is discussed.

5.3.1. Wellhead structure's displacement response with different convection coefficients

The convective heat transfer coefficient (f) are adopted as 0.1 kW m^{-2} K^{-1}, 1.5 kW m^{-2} K^{-1}, and 3 kW m^{-2} K^{-1}. The pressure load on the upper end face of the metal sealing pressure ring ($F1$) are 100 MPa, and the gravitational load of the casing ($F2$) is 154 MPa. The influence of different convective heat transfer coefficients on the displacement of the wellhead structure is analyzed when the node temperature in the model reached a specified value (925 °C in this study), as shown in Fig. 14. As shown in Fig. 14, the vertical displacement in the U_2 direction at the upper end face of the wellhead is the largest (indicated by the bright red area), while the displacement at the bottom of the wellhead is the smallest (blue area). For the wellhead, the vertical displacement in the U_2 direction gradually decreases from top to bottom. The sealing structure and the casing hanger exhibit similar vertical displacements in the U_2 direction. Additionally, the vertical displacement of the casing hanger decreases from top to bottom. Comparing the contour plots in Fig. 14, it is evident that as the convective heat transfer coefficient f increases, the vertical displacement in the U_2 direction of the wellhead and internal structures gradually decreases. However, the change in wellhead displacement is minimal. For instance, when f increases from 0.1 kW m^{-2} K^{-1} to 3 kW m^{-2} K^{-1}, the maximum vertical displacement at the top of the wellhead decreases by only 0.5%. In contrast, for the casing hanger, as f increases from 0.1 kW m^{-2} K^{-1} to 1.5 kW m^{-2} K^{-1}, its displacement decreases significantly; but when f increases from 1.5 kW m^{-2} K^{-1} to 2 kW m^{-2} K^{-1}, the displacement changes little. The reason is once f increases to a certain value, the inner wall temperature of the casing approaches the gas temperature and further increases in f have minimal effect on the inner wall temperature, resulting in negligible changes in displacement response.

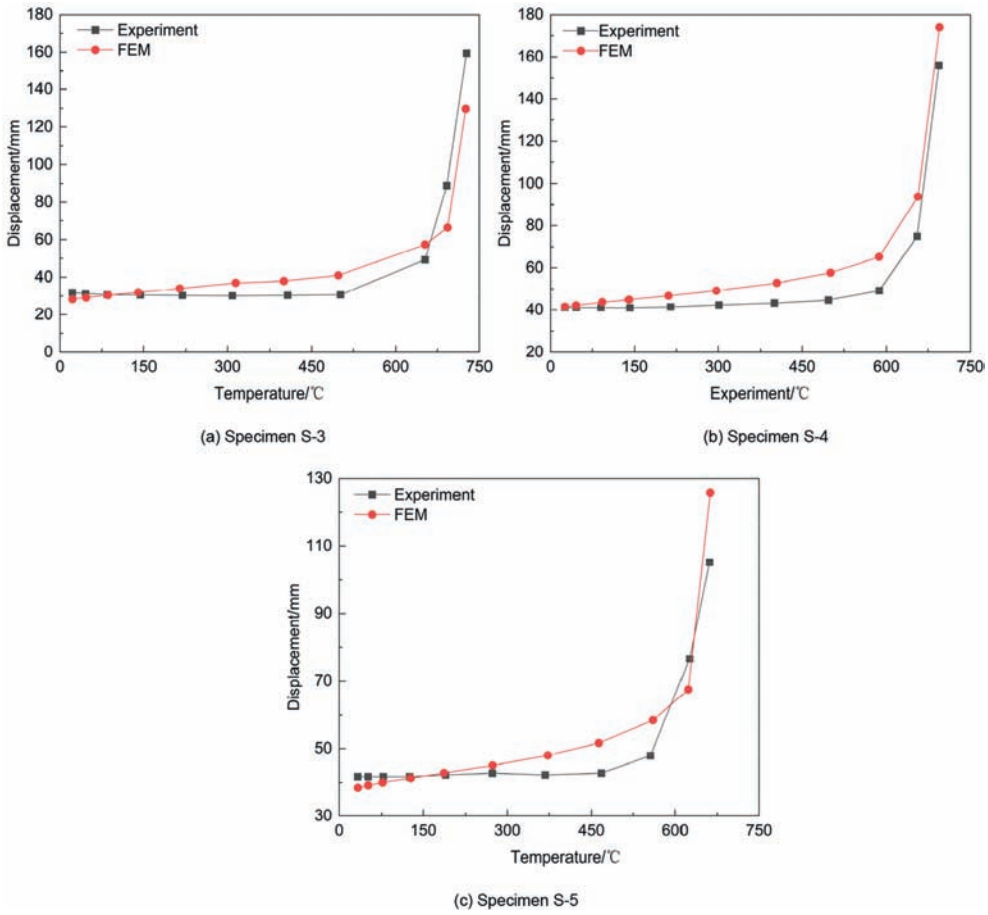


Fig. 13. Experimental and simulation result's for steel beam's displacement.

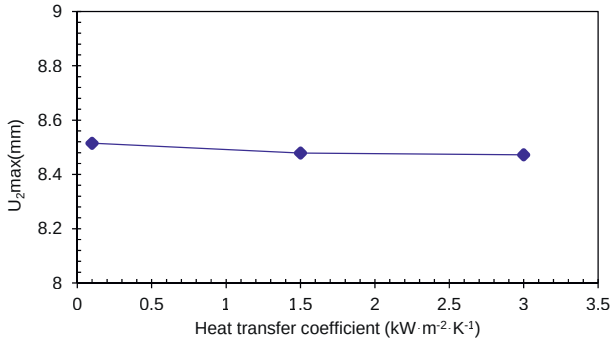


Fig. 14. Wellhead structure's displacement response with convection coefficients.

5.3.2. *Wellhead structure's displacement response with pressure load*

The convective heat transfer coefficient (f) is 0.1 kW m^{-2} K^{-1}; The pressure load (F_1) on the upper end face of the metal sealing pressure ring is 50 MPa, 100 MPa, and 150 MPa; The gravity load of the casing (F_2) is 230 MPa. When the temperature of the analysis model node reaches a certain value (925 °C in this study), the influence law of F_1 on the displacement of the wellhead structure is shown in Fig. 15. As shown in Fig. 15, with F_1 increasing, the displacement of the wellhead structure U2 decreases, but the degree of decrease is relatively small. For the wellhead, as F_1 increases from 50 MPa to 150 MPa, the maximum displacement of the wellhead decreases from 8.52 mm to 8.48 mm, a decrease of only 0.4%. For the casing hanger and sealing device, as F_1 increases from 50 MPa to 150 MPa, the vertical displacement of the casing hanger and metal sealing device changes very little.

5.3.3. *Wellhead structure's displacement response with casing load*

The f is 0.1 kW m^{-2} K^{-1}; F_1 is 100 MPa; F_2 is 153 MP, 230 MPa, and 307 MPa. When the temperature of the analysis model node reaches a certain value (925 °C in this article), the influence of F_2 on the displacement of the wellhead structure is shown in Fig. 16. As shown in Fig. 16, with the increase of F_2, the displacement of the internal structure U2 of the wellhead gradually decreases, but the decrease is relatively small. For the wellhead, with the increase of F_2 from 153 MPa to 307 MPa, the maximum vertical displacement of the wellhead decreased from 8.52 mm to 8.49 mm, a decrease of only 0.32%. As F_2 increases from 153 MPa to 307 MPa, the displacement changes of the casing hanger and the metal sealing device are very small.

5.4. *Wellhead structure fire's resistance limit analysis under well blowout fires*

The criterion for determining whether the structure has reached the fire resistance limit is that the vertical deformation of the structure (U2 displacement direction) reaches 1% of the length of the structure exposed to the fire (Lv, 2018). The fire exposure height of the wellhead in this study is 850 mm, and the wellhead

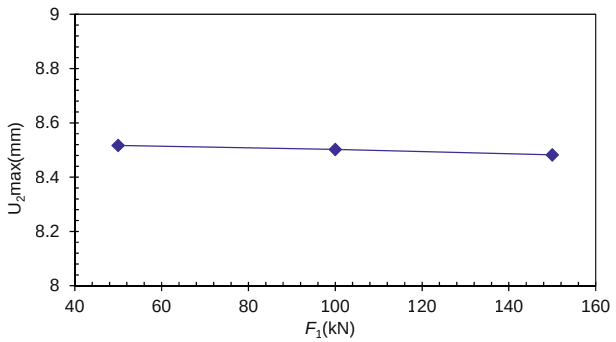


Fig. 15. Wellhead structure's displacement response with pressure load.

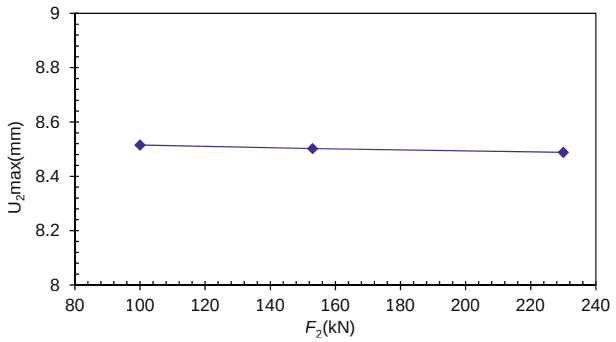


Fig. 16. Wellhead structure's displacement response with casing loads.

reaches the fire resistance limit when the vertical displacement reaches 8.5 mm; Based on the displacement response analysis of the wellhead structure under high temperature in the previous section, the maximum displacement is located at the top of the wellhead, and the vertical displacement of the casing hanger and sealing device is smaller than that of the wellhead. Therefore, the top of the wellhead in the entire structure reaches the fire resistance limit first.

5.4.1. Wellhead structure's fire resistance limit without clearance operations at the well site

The convective heat transfer coefficient is varied at 0.1 kW m^{-2} K^{-1}, 1.5 kW m^{-2} K^{-1}, 3 kW m^{-2} K^{-1}, 6 kW m^{-2} K^{-1}, and 9 kW m^{-2} K^{-1}.The pressure load on the upper end face of the sealing pressure ring (F_1)is 50 MPa, 100 MPa, and 150 MPa, while the gravity load of the casing (F_2)is considered at 154 MPa, 230 MPa, and 307 MPa. The fire resistance limit of the wellhead structure is analyzed under these parameters, as shown in Fig. 17. As depicted in Fig. 17, the fire resistance limit remains relatively constant, fluctuating around 45 min, regardless of the increase in those parameters. This indicates that the fire resistance limit of the wellhead is minimally influenced by those parameters. The reason is that the fire resistance limit pertains to the top of the wellhead, where neither the casing load nor the pressure on the sealing pressure ring's end face directly affect the wellhead top. Furthermore, from the temperature field analysis in the previous section, it is clear that the convective heat transfer coefficient has little impact on the temperature of the wellhead top and the fire-exposed surface (outer surface of the wellhead). The displacement of the wellhead top is primarily influenced by temperature, and the small variations in temperature result in only minor changes in reaching the fire resistance limit. The temperature on wellhead structural mechanical response fundamentally stems from its significant effect on the key mechanical properties of the material. As temperature increases, the elastic modulus and yield strength of the wellhead materials decrease, resulting in reduced structural stiffness and a greater tendency for large deformations.

5.4.2. Wellhead structure's fire resistance limit with clearance operations at the well site

With clearance operations at the well site, the heat source of wellhead structure is the thermal radiation released by well blowout flame. The analysis of the previous section shows that the convection heat transfer coefficient, casing load and pressure load on the upper end face of the metal seal compression ring have little impact on the fire resistance limit of the structure. Therefore, the influence of the heat radiation value of the wellhead on the fire resistance limit of the wellhead structure is mainly discussed. The heat radiation is 6 kW m^{-2}、10 kW m^{-2}、14 kW m^{-2}、18 kW m^{-2}、22 kW m^{-2} and 30 kW m^{-2}; The fluid temperature is 50 °C; Convection heat transfer coefficient is 1.5 kW m^{-2} K^{-1}. Under different thermal radiation, when the wellhead structure temperature tends to be stable, the maximum vertical displacement and maximum temperature of the wellhead structure are shown in Fig. 18.

The maximum vertical displacement of the wellhead occurs at the top of the wellhead similar to the previous section. It can be seen from Fig. 18 that the maximum vertical displacement and

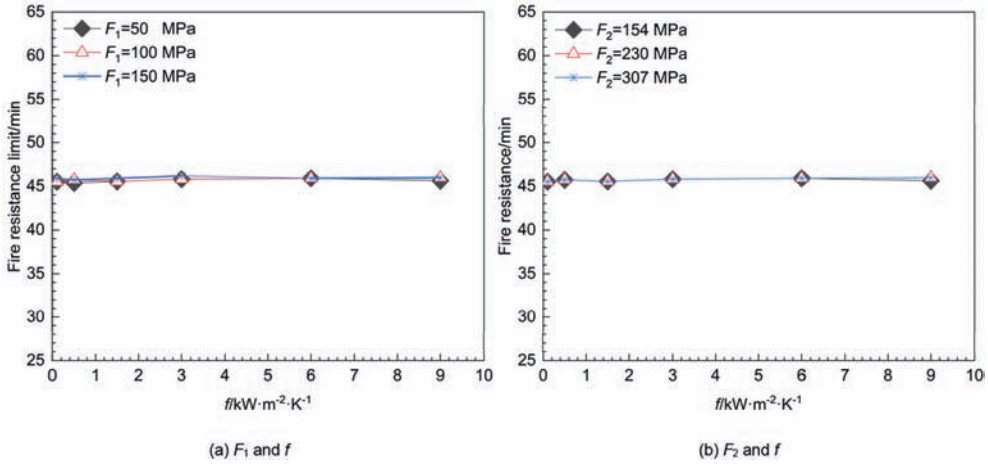


Fig. 17. Effect of different parameters on the fire resistance limit of wellhead structures.

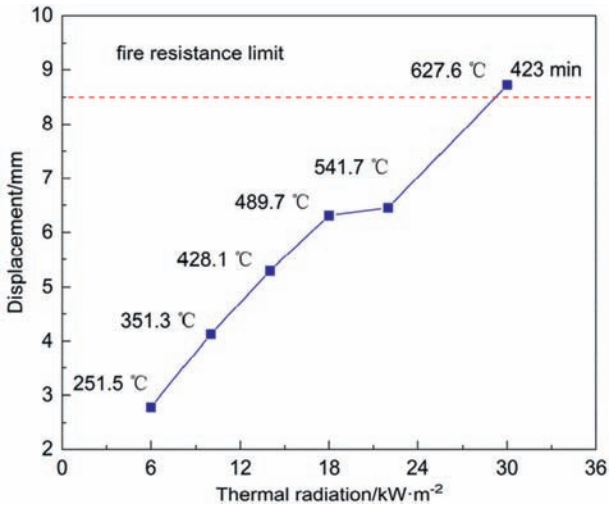


Fig. 18. Wellhead displacement response and fire resistance limit under thermal radiation.

maximum temperature of the wellhead gradually increase with the increase of thermal radiation; When the radiation value is $\leq$ 22 kW m^{-2}, the vertical displacement of the wellhead is less than the corresponding displacement (8.5 mm) of the fire resistance limit; When the radiation value = 30 kW m^{-2}, the vertical displacement of the wellhead is greater than the corresponding displacement of the fire resistance limit, and the time to reach the fire resistance limit is 423 min.

In summary, there is a threshold for the thermal radiation with clearance operations at the well site. When the thermal radiation value exceeds the threshold, the wellhead structure reaches its fire resistance limit, which differs from the condition of clearance operations. In addition, the time for the wellhead to reach the fire resistance limit after clearing is much longer than that before clearing. The main reason is that with clearance operations, the thermal source is the thermal radiation released by the blowout flame, and the thermal radiation value change the wellhead temperature with the influence of the blowout flow rate and other factors. Therefore, the wellhead temperature with clearance operations is lower than the temperature generated by the flame directly acting on the wellhead surface without clearance operations. Therefore, clear the wellhead in time after the blowout fire, which can reduce the risk of the wellhead structure reaching the fire resistance limit, thus reducing the damage of the flame's high temperature to the wellhead structure.

6. Conclusion

Experiments were conducted to investigate the mechanical properties of wellhead materials under high-temperature conditions. Subsequently, based on thermo-mechanical coupling methods, a temperature field model and a mechanical response model of the wellhead structure under fire conditions were established and validated, respectively. The main conclusions were as follows:

(1) With clearance operations at the well site, a thermal radiation threshold existed; Only when the thermal radiation exceeded this threshold, wellhead reached its fire resistance limit and failed. Without clearance operations at the well site, the wellhead structure was certain to reach its fire resistance limit and ultimately fail. Therefore, timely removal of barriers around the wellhead can reduce the risk of reaching the fire resistance limit of the wellhead structure, thereby reducing the damage caused by high flame temperature. The convective heat transfer coefficient, the pressure load on the upper end face of the metal seal pressure ring, and the gravity load of the casing have a negligible effect on the fire resistance limit of the wellhead structure.

(2) Without clearance operations on the well site, the temperature of the wellhead surface is close to the flame temperature, and the rubber seal position temperature reaches its decomposition and failure temperature. The temperature of the outer surface of the wellbore is the highest, and the farther away from the outer surface, the lower the temperature.

(3) A temperature field model and a mechanical response model of the wellhead structure exposed to the gas well blowout fire are established, and the established models can reasonably reflect the experimental results.

(4) With the temperature increase, the stress value, elastic modulus, yield strength, tensile strength and ultimate load of casing and wellhead materials under the same strain gradually decrease, while the elongation gradually increases.

CRediT authorship contribution statement

Yudan Peng: Writing – original draft, Methodology. **Guodong Ji :** Data curation. **Weifeng Chen:** Resources. **Binhui Liu:** Software. **Chen Hao:** Validation. **Wenqiang Lou:** Resources. **Guangming Fu:** Supervision. **Jiying Chen:** Data curation.

Declaration of competing interest

The authors declare that they have no known competing financial interests or personal relationships that could have appeared to influence the work reported in this paper.

Acknowledgments

This work was supported by the National Natural Science Foundation of China [5228810005]. Youth Fund of CNPC Engineering Technology R&D Company Limited [CPETQ202405].

References

Blandford, R.K., Morton, D.K., Snow, S.D., et al., 2007. Tensile stress-strain results for 304L and 316L stainless steel plate at temperature. In: Proceedings of the ASME Pressure Vessels and Piping Conference. ASME, Texas, pp. 617–628.

CEN (European Committee for Standardization), 2005. EN1993-1-2:2005. Eurocode 3: Design of Steel Structures. Part 1-2: General rules- Structural Fire Design.

Duan, J.T., Shi, D.D., Wang, J.H., Y, Jiao, He, P.S., 2017. A study of thermal-mechanical coupled method of analyzing steel structures thermal response in fire based on FDS-ABAQUS. Eng. Mech. 34 (2), 197–206.

Fan, S., Ding, X., Sun, W., 2016. Experimental investigation on fire resistance of stainless steel columns with square hollow section. Thin-Walled Struct. 98, 196–211.

Fang, Q.H., 2006. Study on Mechanical Characteristics of fiber-reinforced Rubber at Different Temperatures. Northeastern University, Shenyang.

Foroughi, V., Palacios, A., Barraza, C., et al., 2021. Thermal effects of a sonic jet fire impingement on a pipe. J. Loss Prev. Process. Ind. 71, 104449.

Ge, Y., 2012. Study on Fire Resistance of Restrained High Strength Q460 Steel Column. Chongqing University, Chongqing.

Gibbs, T.W., Wyatt, H.W., 1961. Short-time tensile properties of type 316 stainless steel at very high temperatures. J. Basic Eng. 83 (4), 481–488.

Hao, J.K., 2020. Thermodynamic Response and Ultimate Strength of Deck Grillage Exposed to Fire. Shanghai Jiao Tong University, Shanghai.

He, B.B., 2018. Research on Fire Resistance Performance of rec-section q550 high-strength Steel Columns with Axial Compression. Southeast University, Nanjing.

He, A., Liang, Y., Zhao, O., 2019. Experimental and numerical studies of austenitic

stainless steel CHS stub columns after exposed to elevated temperatures. J. Constr. Steel Res. 154, 293–305.
He, A., Li, H.T., Lan, X., Liang, Y., Zhao, O., 2020a. Flexural buckling behaviour and residual strengths of stainless steel CHS columns after exposure to fire. Thin-Walled Struct. 152, 106715.
He, A., Liang, Y., Zhao, O., 2020b. Behaviour and residual compression resistances of circular high strength concrete-filled stainless steel tube (HCFSST) stub columns after exposure to fire. Eng. Struct. 203, 109897.
Li, Z.N., 2015. Experimental Investigation of Restrained Axial Compression Stainless Steel Columns at Elevated Temperatures. Southeast University, Nanjing.
Lu, M.C., 2021. Study on Fire Resistance of Concrete Filled Double Skin Steel Tubular Under the Whole Process of Fire. Shenyang University, Shenyang.
Luo, Z., Liang, H., Wang, T., Cheng, F., Su, B., Liu, L., Liu, B., 2021. Evaluating the effect of multiple flammable gases on the flammability limit of ch4: experimental study and theoretical calculation. Process Saf. Environ. Prot. 146, 369–376.
Lv, X., 2018. Residual Load Capacity and Experimental Research on Short Steel Tube Infilled with High Strength Concrete Column Post-fire. Southeast University, Nanjing.
Ma, Y.H., 2018. Research on Shear Performance of Rc Continuous Beam Under Fire. North China University of Science and Technology, Tangshan.
Qi, Y.Q., 2011. Nonliner Finite Element Analysis Research of Reinforced Concrete Structure in Fire. South China University of Technology, Guangzhou.
Rodrigues, J.P.C., Laím, L., 2019. Comparing fire behaviour of restrained hollow stainless steel with carbon steel columns. J. Constr. Steel Res. 153, 449–458.
Sheng, H.H., 2021. Behaviors of Axially Loaded Tubed Steel Reinforced Concrete Stub Column Safter Exposure to Fire. Harbin Institute of Technology, Harbin.
Shi, Y.X., Liu, F., 2019. Analysis of temperature field in drilling four connections under blowout and fire conditions. Petrochem. Technol. 26 (6), 127–128.
Sun, W.X., 2016. Investigation on Fire Resistance of Stainless Steel Columns with Axial Restraint Under Eccentric Compression Loads. Southeast University, Nanjing.
Tondini, N., Rossi, B., Franssen, J.M., 2013. Experimental investigation on ferritic stainless steel columns in fire. Fire Saf. J. 62, 238–248.
Wang, X.Q., 2021. Studies on Behaviour of Axially Loaded Square Tubed Steel Reinforced Concrete Columns After Fire Exposure. Harbin Institute of Technology, Harbin.
Wang, L., Guan, Q.S., 2019. Experimental research on mechanical properties of rubber used for isolation rubber bearings after being subjected to high temperature. Ind. Constr. (8), 7.
Wang, L.L., Qiao, H.Y., 2020. Residual strength assessment of defective pipes under high temperature in fire. J. Xuzhou Inst. Technol. (Nat. Sci. Ed.) 35 (2), 55–59.
Xia, Y., 2018. Study on Fire Resistance of Axially Restrained High Strength Q690 Steel Columns. Chongqing University, Chongqing.
Yu, J.P., 2019. Study on Shear Behavior of Reinforced Concrete Continuous Beams Under Different Fire Conditions. North China University of Science and Technology, Tangshan.
Zhang, X.Q., 2019. Full-scale heat-flow-solid strength calculation and safety assessment of thermal wellhead equipment. Oil Field Equip. 48 (3), 12–18.
Zhang, Y.H., 2022. Experimental Study on Fire Response of Restrained Q960 Steel Beam. Chongqing University, Chongqing.
Zhou, Y.P., 2015. Research on Fire Resistance of Building Seismic Rubber Bearings. Southeast University, Nanjing.
Zhou, Y., Li, Y., Jiang, H., Zhang, K., Chen, X., Huang, L., Gao, W., 2021. Investigations on unconfined large-scale methane explosion with the effects of scale and obstacles. Process Saf. Environ. Prot. 155, 1–10.
Zhou, N., Yun, S.B., Li, X., et al., 2023. Numerical simulation of thermal response of petrochemical pipe gallery under pool fire environment. Ind. Saf. Environ. Prot. 49 (3), 1–6.